A Simple Synthesis Method of Zeolitic Imidazolate Framework-8 (ZIF-8) Nanocrystals as Superior Electrode Material for Energy Storage Systems

Article *in* Journal of Inorganic and Organometallic Polymers and Materials · September 2022

DOI: 10.1007/s10904-022-02475-x

CITATIONS
29

READS
869

5 authors, including:

Siva Vadivel
Karpagam Academy of Higher Education
25 PUBLICATIONS **396** CITATIONS
SEE PROFILE

Murugan Anbazhagan
Kalasalingam Academy of Research and Education
62 PUBLICATIONS **821** CITATIONS
SEE PROFILE

A. Shameem
Karpagam Academy of Higher Education
82 PUBLICATIONS **1,371** CITATIONS
SEE PROFILE

Thangarasu Subramanian
Kalasalingam Academy of Research and Education
45 PUBLICATIONS **388** CITATIONS
SEE PROFILE

Journal of Inorganic and Organometallic Polymers and Materials
https://doi.org/10.1007/s10904-022-02475-x

A Simple Synthesis Method of Zeolitic Imidazolate Framework-8 (ZIF-8) Nanocrystals as Superior Electrode Material for Energy Storage Systems

V. Siva[1] · A. Murugan[2,3] · A. Shameem[1] · S. Thangarasu[2,3] · S. Asath Bahadur[2,3]

Received: 11 May 2022 / Accepted: 17 August 2022

Abstract
A hybrid material, Zeolitic imidazolate frameworks (ZIFs) characterize a kind of new and specialized sort of metal–organic frameworks (MOFs) with imidazole linkers and metal ions with standard aluminosilicate zeolite structure. Their intrinsic pore size, robust functions and high-quality thermal and chemical stability have ended in a huge range of capabilities for diverse ZIF substances. In this promptly increasing area, over the past few years, energetic research activities have emerged from package approaches to potential applications. Herein, a simple method for the preparation of Zeolitic imidazolate framework-8 (ZIF-8) nanocrystals (NCs) has been synthesized by a simple one-step chemical method with starting material such as 2-methylimidazole and Zinc nitrate hexahydrate in methanol solution. Structural, functional, surface morphological and electrochemical performances have been systematically investigated by various analytical techniques. Electrochemical test results show its specific capacitance up to 111.23 F g^{-1} at current density of 1 A g^{-1} in a 3 M KOH electrolyte. In particular, the compound exhibits good cyclic stability with 85.36% capacity retention after 5000 cycles at a given current density of 3 A g^{-1}.

Keywords Metal–organic frameworks · Zeolitic imidazolate framework-8 · Supercapacitors · Charge/discharge · Electrode material

1 Introduction

For a long time, porous materials have been the focus of continuous research not only in basic studies but also in real-world applications due to their essential properties such as huge pore volume, large surface areas and tuneable optical properties. Nevertheless, metal–organic frameworks (MOFs) are deliberated a new area of research, and the hybrid nature of organic–inorganic parts has been widely observed by scientists [1–4]. MOFs are used for interdisciplinary applications due to their remarkable properties such as porous nature, cell volume, huge surface area and bio-degradability. From the aforesaid evidence, the uses of MOFs are also superfluous, including gas/molecular separation, chromatography, fuel cells, drug storage/delivery, sensor and imaging. These MOFs are widely used for many important applications due to their special structural features and thermo-chemical stability [5]. However, a conventional, economical and simple synthesis method in multi-gram scale using a generally accessible tool remains to be explored.

Essentially, Zeolitic imidazolate frameworks (ZIFs) are a new kind of hybrid material with a zeolite topological structure. Their intrinsic pore properties, numerous functions and exceptional thermal and chemical stability have led to an extensive variety of potential applications for various Zeolitic materials [6–9]. ZIFs are special types of MOFs made up of metal ions such as zinc (Zn^{2+}) or cobalt (Co^{2+}) with structures similar to zeolites and these metals are bound by N atoms of imidazole ligands [10, 11]. In recent years, ZIFs with a large specific area, superior pore structure and numerous

✉ V. Siva
siva33phy@gmail.com

1 Department of Physics, Karpagam Academy of Higher Education, Coimbatore, Tamil Nadu 641 021, India

2 Department of Physics, School of Advanced Sciences, Kalasalingam Academy of Research and Education, Krishnankoil, Tamil Nadu 626 126, India

3 Condensed Matter Physics Laboratory, International Research Centre, Kalasalingam Academy of Research and Education, Krishnankoil, Tamil Nadu 626 126, India

Published online: 04 September 2022

surface functional groups have shown great potential in different fields [12]. ZIF-8 is a MOF of all ZIFs, with Zn^{2+} being the metal core and 2-methylimidazole (Hmim) as ligand. It reveals a sodalite topography with 1.6 nm cages and 0.34 nm window size. Numerous studies have been accompanied focusing on the synthesis of nano-scale ZIF-8 crystals with various optimal conditions such as temperature, solvent, reaction time, and energy source [13]. In particular, ZIF-8 has excellent properties such as large pore size (diameter of 11.6 Å), large surface area (1413 m^2/g), high thermal stability (up to 550 °C), and significant chemical resistance to boiling alkaline water and organic solvents.

Research is rapidly focusing on energy conservation and storage from renewable energy sources, with public concern about sustainability evolution and energy crisis in civilization [14–16]. In recent days, supercapacitors (SCs), also known as electrochemical capacitors, have received widespread attention due to their long cycle life, high energy density, reasonable operational safety, and high charge–discharge rate. With relatively high energy density, exceptional cyclic life and reliability, supercapacitors are used in a variety of applications such as hybrid electric vehicles, military, flexible wearable electronic, biomedical and healthcare instruments [17]. Therefore, very helpful in achieving numerous micropores in ZIFs with large specific surface area and consequently provide high specific capacitance.

In this present research work, a facile synthesized ZIF-8 electrode at room temperature without any additives in methanol solution are presented as an efficient potential candidate for energy storage application. The synthesized ZIF-8 was characterized by PXRD, FTIR, SEM–EDS and electrochemical study. Electrochemical tests reveal that the as-prepared nanoscale material provides outstanding specific capacitance and cyclic stability at high current density due to its nanohetero structure, representative the potential of an alternative electrode in supercapacitors.

2 Materials and Methods

2.1 Materials

All the purchased analytical grade chemicals were used without further purification. 2-methylimidazole (99%) and Zinc nitrate hexahydrate (98%) were purchased from Sigma Aldrich. Methanol was used throughout this work.

2.2 Synthesis of Zeolitic Imidazolate Frameworks-8

Nanostructured ZIF-8 crystals were synthesized according to the procedure reported by Yongyong Zhang research group [18]. Initially, 6.556 g 2-methylimidazole was dissolved in 100 ml of methanol. Then 2.968 g zinc nitrate hexahydrate was dissolved in 100 ml of methanol. Both the clear solution were mixed together and was stirred for 2 h at room temperature under a constant speed of 240 rpm. The white precipitate was obtained, filtered and the precipitated sample of ZIF-8 was thoroughly washed by methanol. After that, the product was dried at a temperature of 80 °C for 6 h. The schematic representation for the synthesis of ZIF-8 nanocrystals is shown in Fig. 1

2.3 Characterization Details

The structural property was examined by powder XRD study with Brucker D8 advance ECO X-ray diffractometer with the 2θ range of 5°–80°. The Shimadzu IR Tracer-100 FTIR spectrometer was used to know the functional groups of the synthesised ZIF-8. Topographical images, elemental

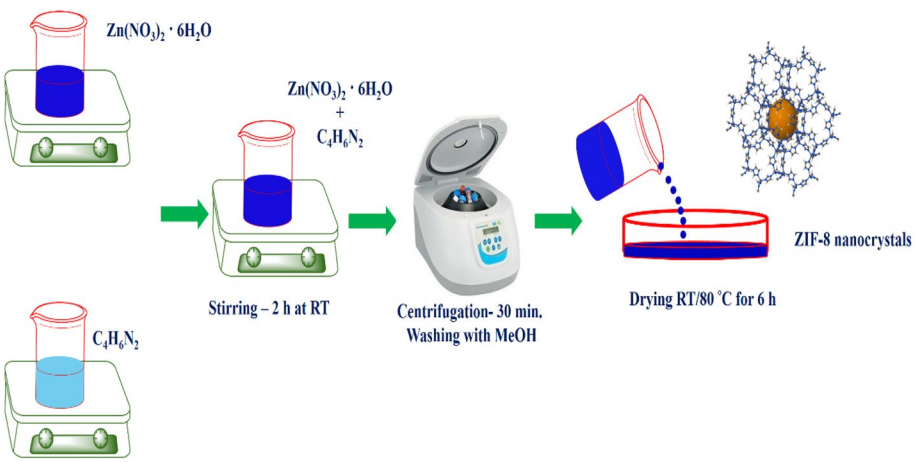

Fig. 1 Schematic representation for synthesis of ZIF-8 nanocrystals

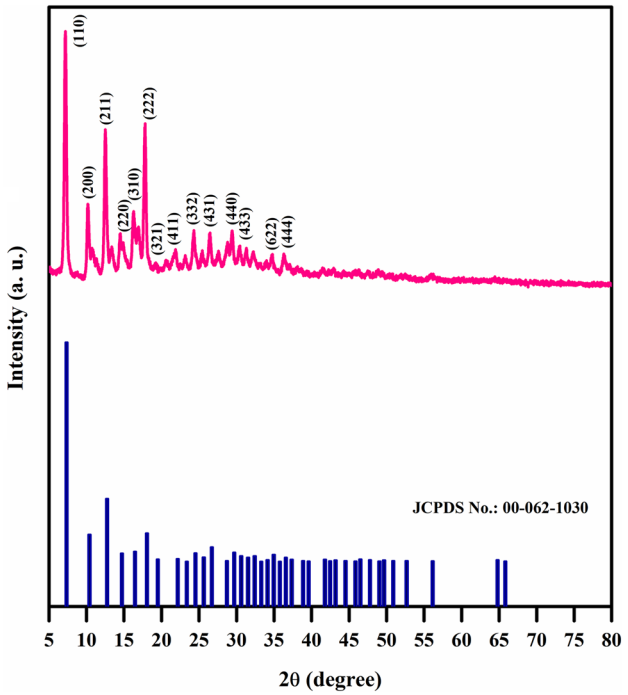

Fig. 2 Powder XRD pattern of ZIF-8 nanocrystals

composition and mapping were investigated by ZEISS-EVO 18 Scanning Electron Microscopy (SEM) attached with EDS. The optical absorption spectrum is recorded in the range between 200 and 1100 nm by Shimadzu 1800 UV visible spectrometer. The electrochemical behaviour of the prepared electrode material was studied by using CHI 6008E electrochemical workstation.

3 Results and Discussion

3.1 Structural Analysis

PXRD analysis is used to investigate the phase purity and structure of synthesised MOF. The XRD pattern of the synthesized ZIF-8 is depicted in Fig. 2. The important characteristic peaks at 2θ = 7.13°, 10.16°,12.58°, 14.53°, 16.25°, 17.81°, 21.98°, 24.31°, 26.49° and 29.26°, which matched to planes such as (110), (200), (211), (220), (310), (222), (321), (411), (332), (431), (440), (433), (622) and (444) respectively. The PXRD pattern exhibits sharp peaks indicates good crystallinity and that well match with the sodalite (SOD) structures of previously published ZIF-8 [18]. There are no additional peaks that are observed which demonstrates the purity of the synthesised ZIF-8. The crystallite size of the synthesised ZIF-8 is calculated through Scherrer's formula [19],

$$\text{Crystallite size}(D) = \frac{0.9\lambda}{\beta Cos\theta} \quad (1)$$

The average crystallite size value is 39 nm calculated for the intensity peaks with corresponding *hkl* plans as (110), (200), (211) and (222).

The functional groups and chemical structure of the synthesised ZIF-8 were confirmed by using FT-IR spectrum and displayed in Fig. 3. It presented remarkable bands at 3411, 3194, 2450, 1573, 1418, 1295, 1142, 992, 753, 679 and 418 cm^{-1}. The band observed at 3411 cm^{-1} was assigned to the N–H stretching vibration of 2-methylimadazole [20–22]. Remarkably, the stretching vibration of Zn-N band is appeared at 418 cm^{-1}, which demonstrates the chemical composition of zinc ions with nitrogen atoms of 2-methylimidazole ligand toward the formation of imidazolate [23]. C–H asymmetric stretching vibrations of the synthesised ZIF-8 are presented at 3194 and 3043 cm^{-1} [24]. A strong band around 1573 cm^{-1} arose from the C=C stretch vibration, while band at 1418 cm^{-1} corresponded to the C=N stretch vibration [18].

3.2 SEM with EDS analyses

SEM analysis is used as an additional tool to determine whether the sample was phase-pure, to confirm the morphology of the ZIFs, and to evaluate the particle size. The surface morphology of the hybrid compound is examined using a scanning electron microscope as shown in the Fig. 4 and its corresponding elemental mapping displayed in Fig. 5, they are uniformly distributed without much accumulation. SEM images with EDS spectrum ensured that the integrated ZIF-8 phase-pure material was similar to the PXRD [18]. These images also indicate that a sodalite topology was developed

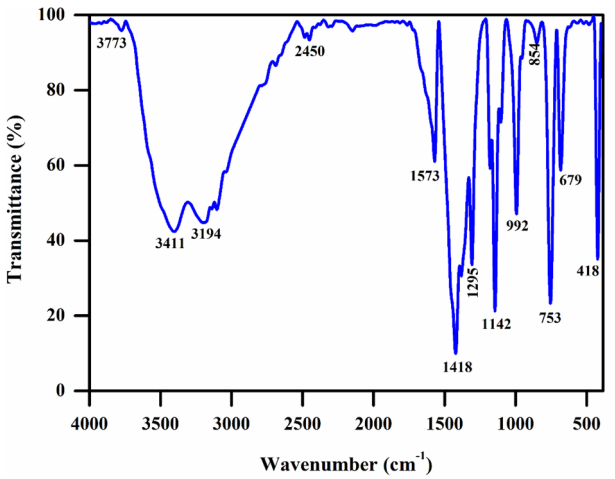

Fig. 3 FTIR spectrum of ZIF-8 NCs

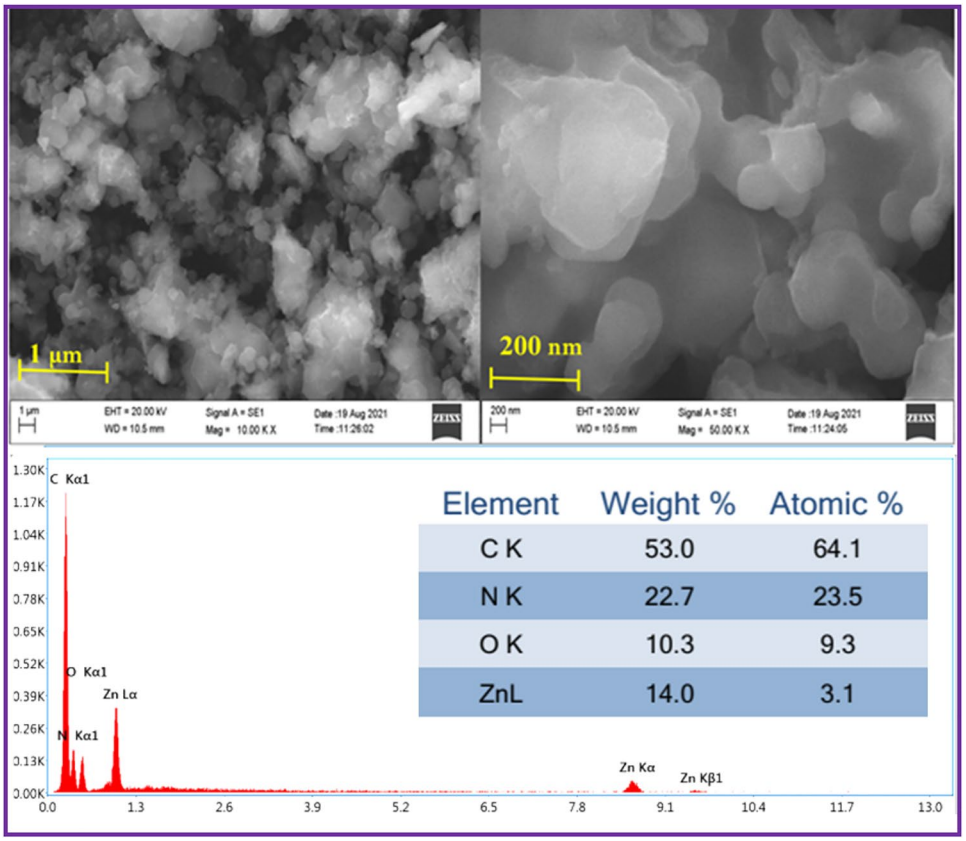

Fig. 4 Topographical images of prepared ZIF-8 material with EDS spectrum (Inset shows in weigh and atomic percentage of the materials)

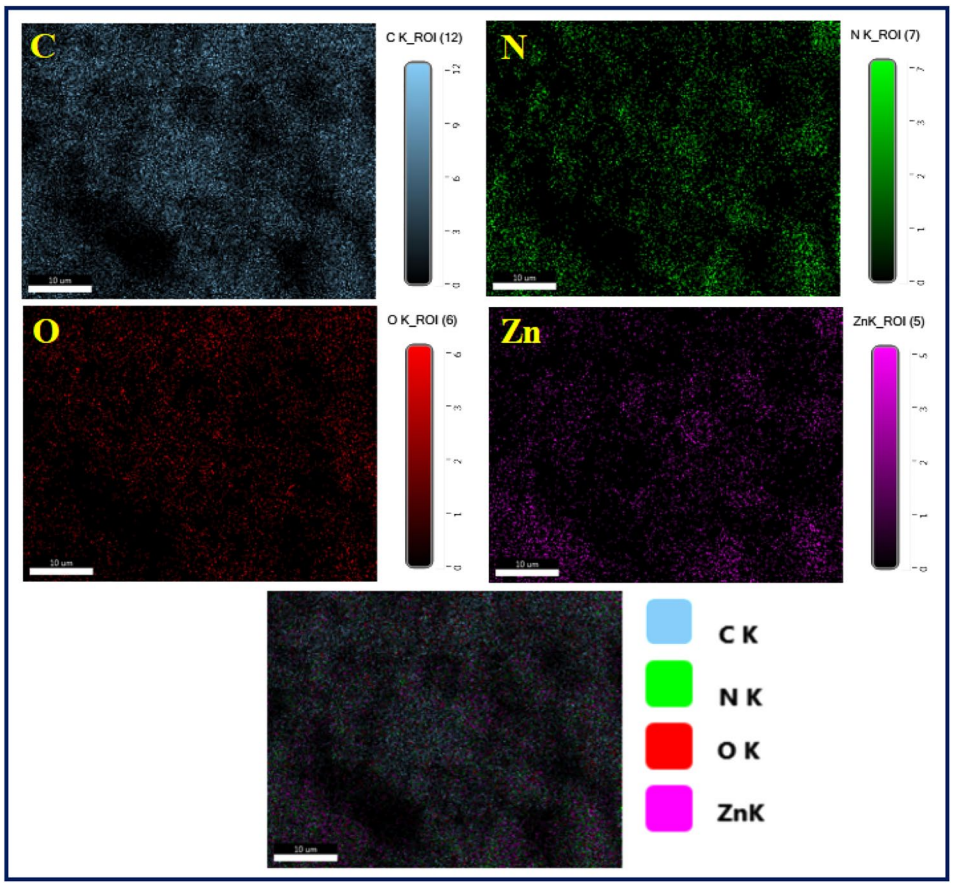

Fig. 5 Elemental mapping for identical element of ZIF-8 nanocrystals

for ZIF-8 (cube). Finally, the diameter of the ZIF-8 particles was approximated. This significant difference in 100 µm diameter is related to the difference specified by the calculated crystallite sizes from PXRD. The corresponding basic maps confirm the presence of a zinc-rich shell in the hollow crystal structures.

3.3 Optical Properties

The optical absorption spectrum is recorded in the range between 200 and 1100 nm and its absorption spectrum is displayed in Fig. 6 (plot for bandgap is given as inset of the Figure). ZIF-8 shows a strong absorption at 208.93 nm. Figure 6 shows that ZIF-8 is an optically transparent MOF with no absorption in the visible region of the spectrum. It shows an absorption edge in deep UV, below 250 nm [25]. The band gap energy is obtained from the Tauc's plot of $(\alpha h\nu)^2$ Vs $(h\nu)$, where, α is the absorption coefficient and h is planck constant. The intercepts of plots on the energy axis confirmed the energy band gaps. From observed inset of the Fig. 6, the band gap value is 5.18 eV and this result is in good agreement with reported in the literature for ZIF-8 [25]. The outcome is suggested that ZIF-8 photoexcited can be performed to create more electron–hole pairs under ultraviolet absorption, which leads to higher photo catalytic performance [26].

3.4 Electrochemical Studies

The as-prepared ZIF-8 material is mixed with polyvinylidene fluoride and acetylene black in a weight ratio of 80:10:10. A little amount of N-methylpyrrolidinone was then added above well mixture active electrode materials and to form a homogeneous slurry. Then the slurry was coated over the nickel foil (1×1 cm^2) substrate by tape-casting technique and dried in vacuum oven at 50 °C for overnight [27]. A three-electrode system consisting of the above ZIF-8 coated materials as a working electrode, platinum (Pt) as a counter electrode and silver/silver chloride (Ag/AgCl) as a reference electrode was used to test the electrochemical performance of the ZIF-8 in 3 M KOH aqueous electrolyte solution. The cyclic voltammetry (CV), galvanostatic charge/discharge (GCD) and electrochemical impedance spectroscopy (EIS) tests were performed on an electrochemical work station. CV and GCD are commonly used to classify the capacitive behavior of modified electrodes [28]. The specific capacitance of the active material is calculated [29] from the following equation,

$$C_{sp(CV)} = \frac{\int IdV}{S \times V \times m} Fg^{-1} \tag{2}$$

$$C_{sp(GCD)} = \frac{I \times t_d}{V \times m} Fg^{-1} \tag{3}$$

$$\eta = \frac{t_d}{t_c} \times 100(\%) \tag{4}$$

where C_{sp} is the specific capacitance (Fg^{-1}) based on the mass of the electroactive materials, $\int IdV$ is the area of oxidation and reduction current (A), V is the window potential (V), 'S' is a analysis different scan rate (mVs^{-1}), 'I' is the applied current (mA), 't_c/t_d' is a charge/discharge time (s) from GCD curve and 'm' is the mass of the electroactive materials in the electrodes (g).

Figure 7a shows the typical CV curves of the ZIF-8 electrode recorded at different scan rate. The CV curves of ZIF-8 electrode at various scan rates of 5 to 150 mV s^{-1} measured between potential window of 0 to 0.6 V in 3 M KOH aqueous electrolyte solution and examined in room temperature [30]. The profiles of the CV curves are obviously shown in non-rectangles, signifying of good charge transmission (redox reaction) at the electrode surface. The redox reaction peaks indicate the pseudocapacitive (Faradic redox reaction) behaviour of ZIF-8 electrode. In addition, as the scan rates increase from 5 to 150 mV s^{-1}, it can be seen that the shapes of these CV curves do not show significant changes, indicating better electron conduction within the electrodes. The electro-chemical reaction of K^+ insertion process [31] taking place at the ZIF-8 electrode can be expressed as.

$$(ZIF-8) + xK^+ + xe^- \leftrightarrow K_x(ZIF-8) \tag{5}$$

where x is the mole fraction of inserted K^+ ions. The specific capacitances were calculated by using Eq. (2). The calculated C_{sp} is 122.47, 120.64, 110.17, 97.43, 85.14,

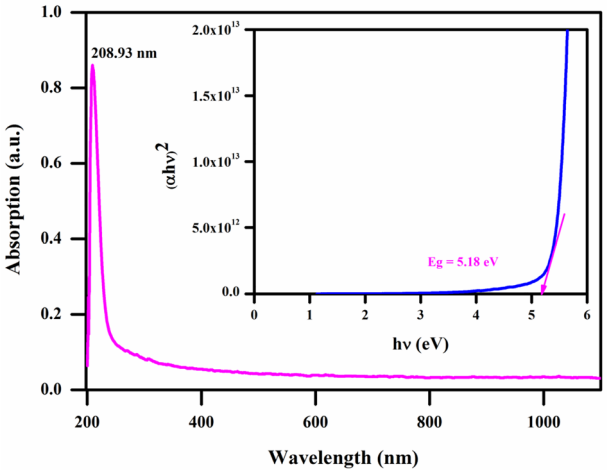

Fig. 6 UV visible spectrum of ZIF-8 nanocrystals

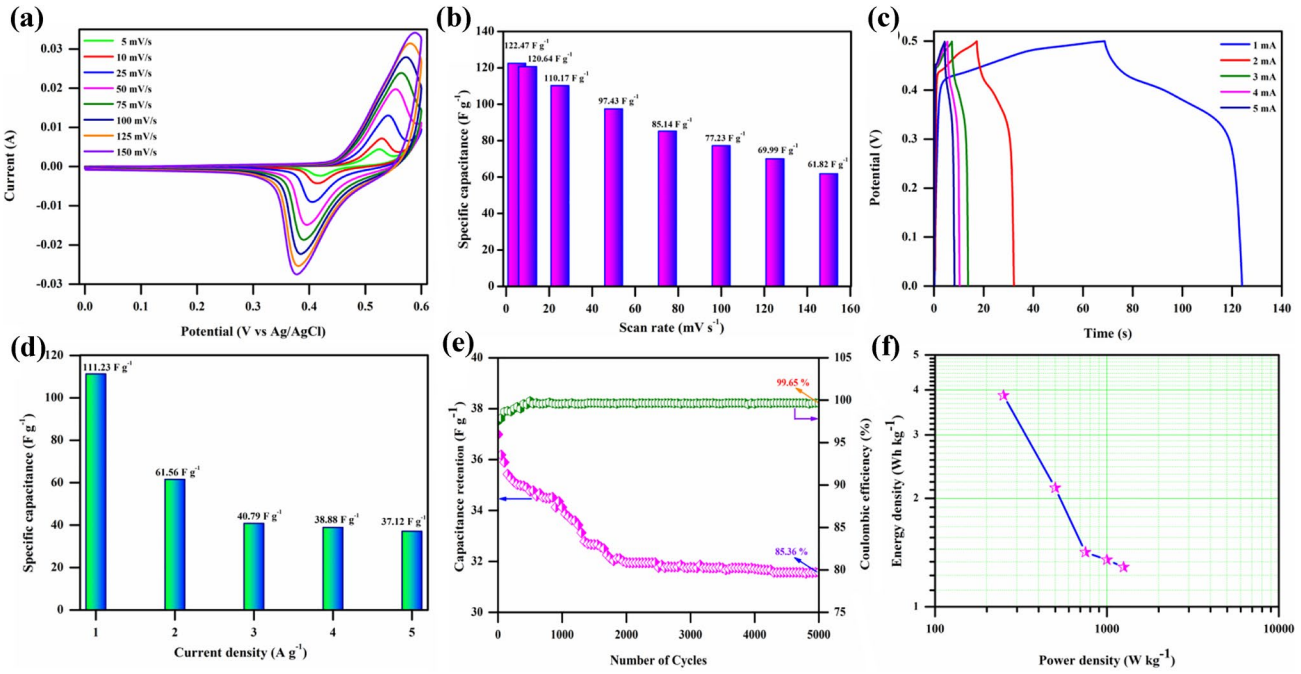

Fig. 7 **a** and **b** are exposed in CV and Csp, **c** and **d** GCD profile and Csp of the MOF materials, **e** Ragone plot and **f** obviously indicated retention of materials up to 5000 cycles for continue charge/discharge cycles with coulombic efficiency

77.23, 69.99 and 61.82 F g^{-1} with respect to scan rate for 5, 10, 25, 50, 75, 100, 125 and 150 mV s^{-1}, respectively. The maximum specific capacitance of 122.47 F g^{-1} was obtained at 5 mV s^{-1} scan rate and this high specific capacitance value increased due to the involvement of ZIF-8 in the Faradic redox reaction. As the scan rate increases the specific capacitance decreases from 122.47 to 61.82 F g^{-1} and the scan rate against the C_{sp} of the modified electrode is shown in Fig. 7b. The reason for the decrease in the reserve capacity of internally active sites that cannot fully retain the redox changes at a high scan rate. This may be due to the diffusion effect of the protons within the electrode. Therefore, ZIF-8 nanostructures assembled from high pores nature of the materials for excellent electrochemical properties, which make them electrode materials that guarantee practical applications [32, 33].

Galvanostatic charge/discharge study was performed to analysis the specific capacitance and to understand the sustainability of this prepared electrode material as supercapacitor electrodes. Figure 7c illustrate the GCD curves are plotted between different current of 1 to 5 mA (Interval is 1 mA). In all charge/discharge curves illustrates the non-rectangle shape is subjective by redox reactions of pseudocapacitor behavior (Faradic redox reaction).The C_{sp} are found to be 111.23, 61.56, 40.79, 38.88 and 37.12 F g^{-1} for 1, 2, 3, 4 and 5 A g^{-1}, respectively. The C_{sp} values were decrease with an increase in the current density from 1 to 5 A g^{-1} (Fig. 7d). At higher current densities, the C_{sp} values gradually decreases, so it is true that the electrode does not have a sufficiently active base [32]. The nonlinear potential variation of charging/discharging profiles shows the pseudocapacitance behavior of electrodes, which results from the redox reaction or electrochemical adsorption/desorption at the interface at certain potentials. The cyclic charge/discharge test is one of the most important aspects of understanding capacitor stability and once-over-life for their useful applications. The electrode material has carried out the analysis up to 5000 cycles of continue charge/discharge examined at 3 mA for evaluate their stability as supercapacitor electrode material. Figure 7e shown in specific capacitance retune with coulombic efficiency plot. The GCD cycles up to 1130 cycles has degraded, after 750 cycles minimum amount was degrade. Decrease in C_{sp} is associated with OH embedding/expulsion of the prepared material. With low current density, the OH diffuses completely inside the material. In contrast, OH is rarely inaccessible and the redox is restricted to the surface, thus reducing efficiency. Loss of continuous charge/discharge cycles up to 1880 cycles was observed at 13.18%. The loss was only 1.46% until 5000 cycles and longer cycling lifetime was revealed. The coulombic efficiency is obtained as 99.65% at after 5000 cycles. Ragone plots are commonly used to compare the performance of various energy saving devices. The power and energy density of electrode materials were calculated from the discharge curves measured at variation of current densities (Fig. 7f).

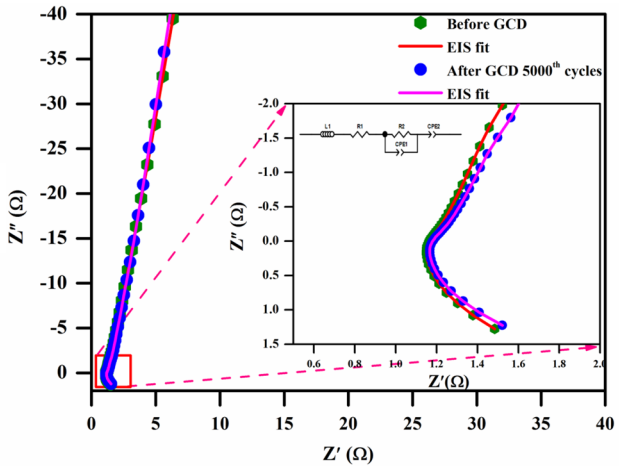

Fig. 8 Electrical impedance spectra of ZIF-8 with inset shows in equivalent circuit

Power density and energy density were calculated using the equation [34].

$$E = \frac{C_{sp} \times \Delta V^2}{7.2} Whkg^{-1} \tag{6}$$

$$P = \frac{E}{t_d} \times 3600 Wkg^{-1} \tag{7}$$

where E and P is energy and power density, Csp is specific capacitance as calculated in GCD (Fg^{-1}), ΔV is potential window (V) and t_d is discharge time (s). The supercapacitor had a high energy density of 3.86 Wh kg^{-1} at 1 Ag^{-1} and high power density is 1250 W kg^{-1} at 5 Ag^{-1}.

The Electrochemical Impedance Spectroscopy analysis was examined in room temperature over the frequency range 1 Hz to 100 kHz and with an applied potential amplitude of 5 mV. The Fig. 8 illustrate that the Nyquist plot of ZIF-8 electrode and inset shown an equivalent circuit. EIS was measured before and after continue charge and discharge of 5000 cycles. The Nyquist plot was shows in dipped semicircle is appearing in high to mid-frequency region and a spike is appeared in low frequency region [34]. Thus, the spike as indicated in diffusion and adsorption of ion in between electrode and electrolyte inter phase. The impedance parameters are analyzed by *Z-view* fitting software and fitted well with the equivalent circuit from the resistance curves measured in the Nyquist plot. Resistance R_s is associated with built-in resistors, including the internal resistance of the electrolyte and the contact resistance developed between the electrode and the current collector. The Fig. 8 is showing a small imperfect semicircle due to the fast ion interaction between the electrode surface and electrolyte. The fitted parameters of R_s and R_{ct} from Nyquist plots are 1.15, 1.17 Ω and 0.83, 0.91 Ω for before and after GCD cycles, respectively. The low value of R_{ct} is represents a higher performance of ZIF-8 electrode [35]. The low-frequency region, the spike nearly vertical trend which is delegate of a higher supercapacitive behaviour of the ZIF-8 electrode [36]. This is because the diffusive process of the electrolyte on the surface of electrode is promoted at low frequencies.

4 Conclusions

The synthesized nanocrystals of Zeolitic imidazolate frameworks-8 were examined as electrode material for supercapacitor application. The synthesized ZIF-8 NCs were explored by physical and electrochemical properties. Structural and functional groups were confirmed by the PXRD and FTIR analyses. UV–visible spectrum showed a strong absorption peak at 208 nm and the band gap about 5.18 eV. The modified electrode was tested on its electrochemical performance of KOH aqueous electrolyte. The introduction of the nanoporous network improves the ion diffusion in the electrode material and leads to a higher specific capacity of 122 F g^{-1} at 5 mVs^{-1}, retaining more than 85.36% capacity after 5000 consecutive charge–discharge cycles. The maximum energy density provided is 3.86 Wh kg^{-1} and the maximum power density is 1250 W kg^{-1}. This high specific capacity interface is confirmed by the low values of charge transfer resistance. Therefore, the electrode can detect potential applications in the field of energy storage systems.

Acknowledgements One of the authors V. Siva is thankful to the Management of Karpagam Academy of Higher Education, Coimbatore-641021, India for financial support under the Seed money scheme (No.: KAHE/R-Acad/A1/Seed Money/004).

Funding The authors have not disclosed any funding.

Declarations

Conflict of interest None.

References

1. Y. Zhao, Z. Song, X. Li, Q. Sun, N. Cheng, S. Lawes, X. Sun, Energy Storage Mater. **2**, 35–62 (2016). https://doi.org/10.1016/j.ensm.2015.11.005
2. K. Wang, K.N. Hui, K.S. Hui, S. Peng, Y. Xu, Chem. Sci. **12**, 5737–5766 (2021). https://doi.org/10.1039/D1SC00095K
3. A.E. Baumann, D.A. Burns, B. Liu et al., Commun. Chem. **2**, 86 (2019). https://doi.org/10.1038/s42004-019-0184-6
4. V. Siva, A. Shameem, A. Murugan, S. Athimoolam, G. Vinitha, S.A. Bahadur, Chin. J. Phys **68**, 764–777 (2020). https://doi.org/10.1016/j.cjph.2020.09.036

5. M. Safaei, M.M. Foroughi, N. Ebrahimpoor, S. Jahani, A. Omidi, M. Khatami, TrAC Trends Anal. Chem. **118**, 401–425 (2019). https://doi.org/10.1016/j.trac.2019.06.007
6. H.N. Abdelhamid, A.P. Mathew, Chem. Eng. J. **426**, 131733 (2021). https://doi.org/10.1016/j.cej.2021.131733
7. H.I. Adil, M.R. Thalji, S.A. Yasin, I.A. Saeed, M.A. Assiri, K.F. Chong, G.A.M. Ali, RSC Adv. **12**, 1433–1450 (2022). https://doi.org/10.1039/D1RA07034G
8. H.N. Abdelhamid, A.P. Mathew, Carbohyd Polymer **274**, 118657, (2021). https://doi.org/10.1016/j.carbpol.2021.118657
9. Y. Shan, M.Y. Zhang, Y. Bai, M. Du, X. Guo, H. Pang, Chem. Eng. J. **429**, 132146 (2022). https://doi.org/10.1016/j.cej.2021.132146
10. K. Noh, J. Lee, J. Kim, Isr. J. Chem. **58**, 1–15 (2018). https://doi.org/10.1002/ijch.201800107
11. A.A. Lourenço, F.F. da Silva, Hetero. Catal. (2022). https://doi.org/10.1016/B978-0-323-85612-6.00017-6
12. T. Thenrajan, S.S. Sankar, G. Srinivasan, S. Kundu, J. Wilson, Dalton Trans. **50**, 10540–10548 (2021). https://doi.org/10.1039/D1DT01718G
13. A.M. Marti, M. Van, K.J. Balkus, J. Porous Mater. **21**, 889–902 (2014). https://doi.org/10.1007/s10934-014-9840-5
14. V. Siva, A. Murugan, A. Shameem, S. Thangarasu, S.A. Bahadur, J. Energ Storage (2022). https://doi.org/10.1016/j.est.2022.103965
15. C.I. Priyadharsini, G. Marimuthu, T. Pazhanivel, P.M. Anbarasan, V. Siva, L. Mohana, J. Sol-Gel Sci. Tech **96**(2), 416–422 (2020). https://doi.org/10.1007/s10971-020-05393-x
16. A. Murugan, V. Siva, A. Shameem, S.A. Bahadur, J. Energy Storage **44**, 103423 (2021). https://doi.org/10.1016/j.est.2021.103423
17. P. Siwatch, K. Sharma, N. Manyani, J. Kang, S.K. Tripathi, J. Alloys Compd. **872**, 159409 (2021). https://doi.org/10.1016/j.jallcom.2021.159409
18. Y. Zhang, Y. Jia, M. Li et al., Sci. Rep. **8**, 9597 (2018). https://doi.org/10.1038/s41598-018-28015-
19. A.A. Tezerjani, R. Halladj, S. Askarib, RSC Adv. **11**, 19914–19923 (2021). https://doi.org/10.1039/D1RA02856A
20. L. Bazzi, I. Ayouch, H. Tachallait, S. EL Hankari, Results Eng. **13**, 100378 (2022). https://doi.org/10.1016/j.rineng.2022.100378
21. H. Erer, O.Z. Yeşilel, O. Büyükgüngör, Polyhedron **29**, 1163–1167 (2010). https://doi.org/10.1016/j.poly.2009.12.017
22. O.L. Rose et al., Nanomaterials **11**, 1367 (2021). https://doi.org/10.3390/nano11061367
23. Y. Zhang, Y. Jia, L. Hou, RSC Adv. **8**, 31471–31477 (2018)
24. M.N. Shahrak, M. Ghahramaninezhad, M. Eydifarash, Environ. Sci. Pollut. Res. **24**, 9624–9634 (2017)
25. N.B. Pulumati, M.B.K. Urs, S. Mandal, B. Vinayak, B. Kamble, AIP Adv. **10**, 085105 (2020). https://doi.org/10.1063/5.0014442
26. T. Wang, Y. Wang, M. Sun, Chem. Sci. **11**, 6670–6681 (2020). https://doi.org/10.1039/D0SC01397H
27. V. Siva, A. Murugan, A. Shameem, S.A. Bahadur, J. Mater, Sci. Mater. Electron. **31**(22), 20472–20484 (2020). https://doi.org/10.1007/s10854-020-04566
28. X. Yang, K. Xu, R. Zou, J. Hu, Nanomicro Lett. **8**, 143–150 (2016). https://doi.org/10.1007/s40820-015-0069-x
29. J.M. Lee, M.E. Briggs, C. Hu, A.I. Cooper, Nano Energy **46**, 277–289 (2018). https://doi.org/10.1016/j.nanoen.2018.01.042
30. X. Liu, H. Xie, J. Mao, J. Electroanal. Chem. **911**, 116228 (2022). https://doi.org/10.1016/j.jelechem.2022.116228
31. K.P. Cheng, R.J. Gu, L.X. Wen, RSC Adv. **10**, 11681–11693 (2020). https://doi.org/10.1039/D0RA01411G
32. Y. Gao, J. Wu, W. Zhang et al., J Solid State Electrochem **18**, 3203–3207 (2014). https://doi.org/10.1007/s10008-014-2578-9
33. R. Kumar, S.M. Youssry, H.M. Soe, M.M. Abdel-Galeil, G. Kawamura, A. Matsuda, J. Energy Storage **30**, 101539 (2020)
34. R. Packiaraj et al., J Energy Storage **34**, 102029 (2021). https://doi.org/10.1016/j.est.2020.102029
35. M. Isacfranklin, R. Yuvakkumar et al., Sci. Rep. **10**(1), 1919 (2020). https://doi.org/10.1038/s41598-020-75879-9
36. L. Wan, E. Shamsaei, C.D. Easton et al., Carbon **121**, 330–336 (2017). https://doi.org/10.1016/j.carbon.2017.06.017